



Mechanical response of nickel–titanium instruments with different cross-sectional designs during shaping of simulated curved canals

H. C. Kim¹, H. J. Kim¹, C. J. Lee², B. M. Kim², J. K. Park¹ & A. Versluis³

¹Department of Conservative Dentistry, School of Dentistry, Pusan National University, Busan; ²Division of Precision Manufacturing Systems, Pusan National University, Busan, Korea; and ³Division of Biomaterials, Department of Restorative Sciences, School of Dentistry, University of Minnesota, Minneapolis, MN, USA

Abstract

Kim HC, Kim HJ, Lee CJ, Kim BM, Park JK, Versluis A.

Mechanical response of nickel–titanium instruments with different cross-sectional designs during shaping of simulated curved canals. *International Endodontic Journal*, 42, 593–602, 2009.

Aim To evaluate how different cross-sectional designs affect stress distribution in nickel–titanium (NiTi) instruments during bending, torsion and simulated shaping of a curved canal.

Methodology Four NiTi rotary instruments with different cross-sectional geometries were selected: ProFile and HeroShaper systems with a common triangle-based cross section, Mtwo with an S-shaped rectangle-based design and NRT with a modified rectangle-based design. The geometries of the selected files were scanned in a micro-CT and three-dimensional finite-element models were created for each system. Stiffness characteristics for each file system were determined in a series of bending and torsional conditions. Canal shaping was simulated by inserting models of the rotating file into a 45° curved canal model. Stress distribution in the instruments was recorded during

simulated shaping. After the instruments were retracted from the canal, residual stresses and permanent bending of their tips due to plastic deformation were determined.

Results The greatest bending and torsional stiffness occurred in the NRT file. During simulated shaping, the instruments with triangle-based cross-sectional geometry had more even stress distributions along their length and had lower stress concentrations than the instruments with rectangle-based cross sections. Higher residual stresses and plastic deformations were found in the Mtwo and NRT with rectangle-based cross-sectional geometries.

Conclusions Nickel–titanium instruments with rectangle-based cross-sectional designs created higher stress differentials during simulated canal shaping and may encounter higher residual stress and plastic deformation than instruments with triangle-based cross sections.

Keywords: cross section, finite element, NiTi file, rectangular, stress distribution, triangular.

Received 30 May 2008; accepted 26 January 2009

Introduction

Nickel–titanium (NiTi) rotary instruments have an important role in root canal preparation (Sattapan

et al. 2000) and enable clinicians to predictably and efficiently create tapered preparations, especially in curved canals (Peters 2004). This ability of NiTi instruments to follow the curvature of a root canal and to cut efficiently is facilitated by its bending and torsional stiffness characteristics. Instruments with increased flexibility cause fewer undesirable changes in the shape of curved canals than those with greater resistance to bending (Thompson & Dummer 1997), whilst increased torsional stiffness transfers rotational

Correspondence: Hyeon-Cheol Kim, DDS, MS, PhD, Department of Conservative Dentistry, School of Dentistry, Pusan National University, 1-10, Ami-dong, Seo-gu, Busan 602-739, Korea (Tel.: +82 51 240 7978; fax: +82 51 254 0575; e-mail: golddent@pusan.ac.kr).

cutting forces more efficiently (da Silva *et al.* 2005, Kim *et al.* 2008, 2009). The effective stiffness characteristics of NiTi instruments are determined by their specific geometrical design (Camps & Pertot 1994, Camps *et al.* 1995, Kazemi *et al.* 2000, Schäfer & Tepel 2001) and cross-sectional geometry in particular has been identified as an important design feature for torsion and bending properties (Camps *et al.* 1995).

As the predictable and efficient instrumentation of curved root canals with NiTi instruments has also led to an increasing use by general practitioners, instrument fractures have become of more concern (Averbach & Kleier 2001). A rotary instrument is subjected to numerous forces, which change constantly during rotation in a canal depending on contact conditions. Instrument fractures have been attributed to torsional fracture and flexural fatigue (Sattapan *et al.* 2000). Torsional fracture occurs when the tip or any part of the instrument becomes locked in a canal whilst the shaft continues to rotate. This leads to a rapid increase in stress levels within the torqued instrument, which will fracture at the location where its material strength is exceeded. Failure due to flexural fatigue occurs in curved canals, because during each rotation the bending direction is reversed causing repetitive stress cycles that can initiate and propagate fatigue cracks. Fatigue cracks lower the structural strength of rotary instruments, which will fail when a critical crack length is reached (Cheung & Darvell 2007a,b, Cheung *et al.* 2007). High cyclic fatigue cracks are accompanied with little plastic deformation around the crack area, and are therefore difficult to detect before the critical crack length is reached. Thus, fatigue failure usually occurs unexpectedly without any prior warning.

Stress concentrations are the most likely locations for fracture and fatigue initiation and avoiding such stress concentrations in instruments should improve fracture performance. Stress levels in rotary instruments depend not only on bending and applied forces, but also on the loading history of an instrument. Accumulated plastic deformation can leave an instrument permanently deformed and introduce so-called residual strains and stresses. This means that strains and stresses are present even when the instrument is not loaded. Cross-sectional geometry is a determining factor in designing favourable stress distributions in NiTi instruments. Several finite-element (FE) studies have shown that the mechanical behaviour of instruments during root canal shaping is directly influenced by their cross-sectional profile (Turpin *et al.* 2000, Berutti *et al.* 2003,

Xu *et al.* 2006). Consequently, various cross-sectional designs have been introduced (Yao *et al.* 2006), such as triangle-based, rectangle-based or S-shaped rectangle-based designs.

The purpose of this study was to evaluate how the cross-sectional designs of four commercial NiTi instruments affected their stress distributions. The selected instruments represented files with triangle-based, S-shaped and rectangle-based cross-sectional designs. To obtain a comprehensive comparison of their mechanical performance, both elastic responses (characterized by stiffness in bending and torsion) and plasticity effects (such as permanent bending and residual stresses) were evaluated. The deformations and stress distributions were determined in a series of basic tests (bending and torsion) and in a simulated curved canal shaping, using three-dimensional FE analysis.

Materials and methods

Four commercially available NiTi rotary instruments with different cross-sectional geometries but comparable sizes were selected for this study: ProFile (Dentsply Maillefer, Ballaigues, Switzerland) and HeroShaper (Micromega, Besançon, France) systems with a common triangle-based cross-sectional design, the Mtwo (VDW, Munich, Germany) system with an S-shaped rectangle-based design and the NRT (MANI, Tochigi, Japan) system with a modified rectangle-based design. The ProFile, HeroShaper and NRT files were of size 30, .06 taper and that of the Mtwo file was of size 30, .05 taper (Fig. 1).

Instrument and canal models

The geometries of the four instruments were obtained using a micro-CT scanner (HMX; X-Tek Group, Santa Clara, CA, USA). The surfaces acquired by the CT-scan were further processed using a three-dimensional modelling program (IDEAS11 NX; UGS, Plano, TX, USA) to suppress noise and refine the definition of the file tips and sharp edges. The file models were meshed in the same software (IDEAS11 NX) using linear, eight-noded hexahedral elements. The final FE model of the ProFile instrument consisted of 7920 elements with 11 940 nodes, the HeroShaper consisted of 6192 elements with 11 299 nodes, the Mtwo consisted of 5300 elements with 7018 nodes and the NRT consisted of 9440 elements with 18 214 nodes. The final FE models of the four NiTi instruments are shown in Fig. 1. The z-axis was chosen along the length of the

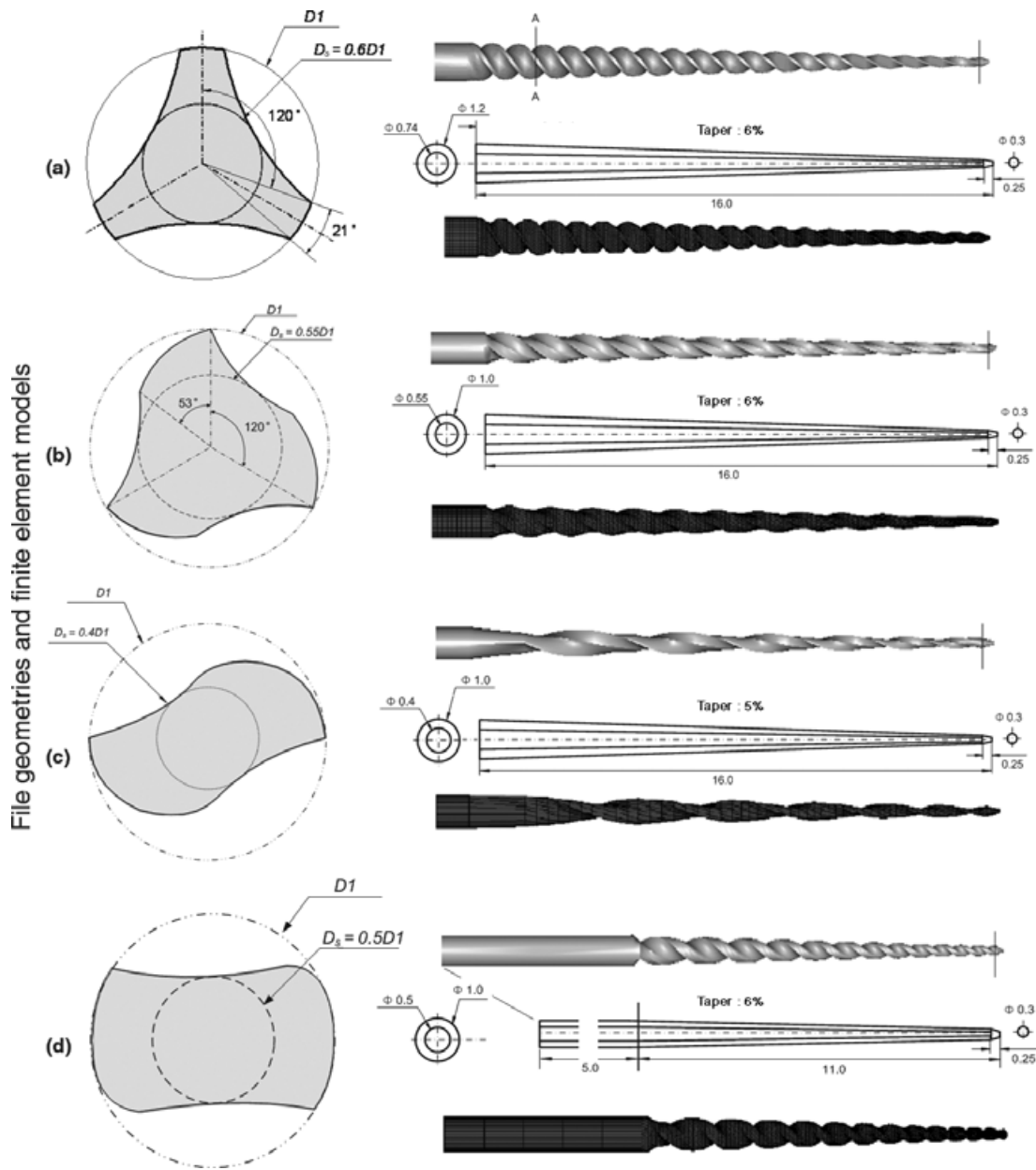


Figure 1 Cross-sectional, longitudinal geometries and finite element models of four NiTi files used in this study. (a) ProFile .06/#30; (b) HeroShaper .06/#30; (c) Mtwo .05/#30; (d) NRT .06/#30.

instruments, i.e. normal to the cross section. Additionally, a 13 mm long curved canal was modelled using plate elements. The canal model had a 0.50 mm diameter apical foramen and approximately 5% apical taper. The simulated canal was designed to be of a larger size than the instrument models to enable rotation inside the canal. Canal curvature was chosen to be approximately 45° (Fig. 2).

Mechanical properties

When a NiTi alloy is stressed, austenite deformation is first elastic, followed by 5% of a pseudoelastic-plateau deformation and martensic phase transformation. The martensic phase deforms elastically until 8% strain, when it becomes plastic. The elastic strain and transformation strain are reversible, but plastic strain is

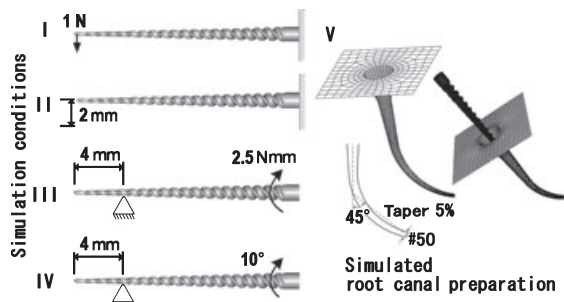


Figure 2 Simulated conditions of I, 1 N loading on file tip; II, 2 mm fixed displacement at file tip; III, 2.5 N mm torsional moment at shaft end; IV, 10°-clockwise rotation of shaft end; and V, insertion and rotation in simulated curved root canal.

irreversible (Xu *et al.* 2006, Wang 2007). The mechanical properties used in this study for the NiTi alloy were a Young's modulus of 36 GPa and a Poisson's ratio of 0.3 (Wang 2007). The critical stress at the beginning of the phase transformation was 504 and 755 MPa at the end.

Numerical analyses

Several numerical experiments were performed to determine the mechanical response and stress distributions in the different file systems using ABAQUS V6.5-1 (SIMULIA, Providence, RI, USA).

Flexure of the instrument tip was measured and the von Mises stress distribution was evaluated when it was deformed by applying a static load of 1 N on the tip of each NiTi instrument, which was fixed at the shaft (Fig. 2, simulation I). A von Mises stress is a so-called equivalent stress, which represents the three-dimensional stress condition with a single value according to the von Mises criterion. In a similar experiment, bending displacement (2 mm) of the instrument tip was simulated to obtain the resulting von Mises stresses and the load (Fig. 2, simulation II).

The instrument was rotated using a torsional moment of 2.5 N mm at the shaft and the von Mises stress distributions were calculated whilst the instruments were clamped rigidly 4 mm from their tip (Fig. 2, simulation III). Additionally, when a 10° clockwise rotation was applied to the shaft (Fig. 2, simulation IV), the von Mises stresses and resulting torque were determined to obtain torsional stiffness.

To evaluate the stress distributions during conditions of root canal shaping, which involves simultaneous cyclic bending and torsion, the instruments

were inserted into the simulated canal model (Fig. 2, simulation V). The simulation started with the instruments at approximately 7 mm from the apical end without rotation, after which they were slowly introduced to make first contact at 6 mm of working length in approximately 0.5 s. The instruments were advanced continuously, without repetitive up and down pecking or brushing movements, to the end of the canal to reach the apex after approximately 1 s. During this insertion, the instruments rotated at 240 rpm (four rotations per second). The canal walls were rigid, whilst the Coulomb friction coefficient between the instruments and canal wall was chosen to be 0.01 to avoid binding during the numerical analysis. Stresses calculated in the instruments were collected during the simulated shaping. After 2 s, the files were removed from the canal to allow elastic recovery and determination of residual stresses due to plastic deformation. von Mises strains of permanent bending of the file tips were determined in the retracted instruments.

Results

Stiffness characteristics

Figure 3 (left) shows the displacement–force curves of the four file systems. As bending stiffness was defined as the force needed for bending deflection, a steeper slope indicates a higher stiffness. The graph shows that the NRT system had the highest bending stiffness, whilst the Mtwo system was the least stiff (i.e. most compliant or flexible). The graph also shows that the stiffness curves were not linear, which was most obvious for the Mtwo file system. It was verified using a linear-elastic analysis that the nonlinearity was attributed mainly to the geometry rather than shape memory alloy phase transformation. Figure 4 illustrates the bending deformation and shows the von Mises stress distributions in a cross section for each instrument type. In simulation I (1 N bending load), the highest maximum von Mises stress value was found in the NRT (706 MPa), followed by the Mtwo (690 MPa), ProFile (577 MPa) and HeroShaper (549 MPa), with corresponding deflections of 3.50, 6.67, 4.59 and 5.59 mm respectively. The maximum von Mises equivalent stress values were found at different locations in the instruments. These were closest to the instrument tip in the Mtwo (2.49 mm), followed by the NRT (3.14 mm), HeroShape (4.10 mm) and ProFile (8.38 mm). In simulation II, under a 2 mm deflection, the highest maximum

Figure 3 Correlation between loads and deformations in bending (left) and torsion (right). A steeper slope indicates a higher stiffness.

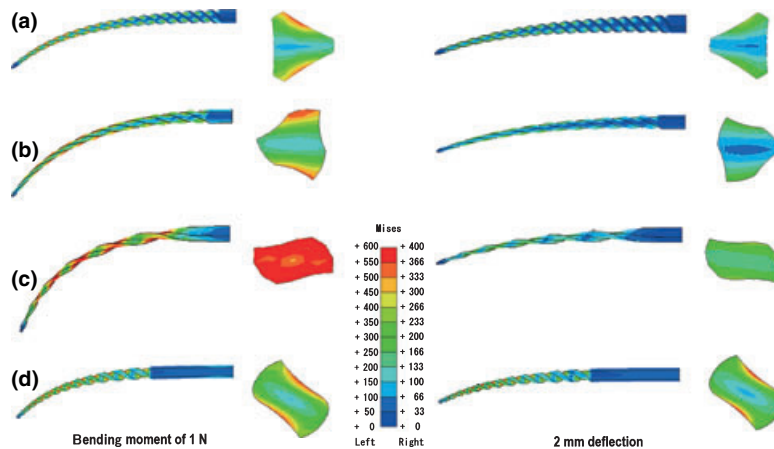
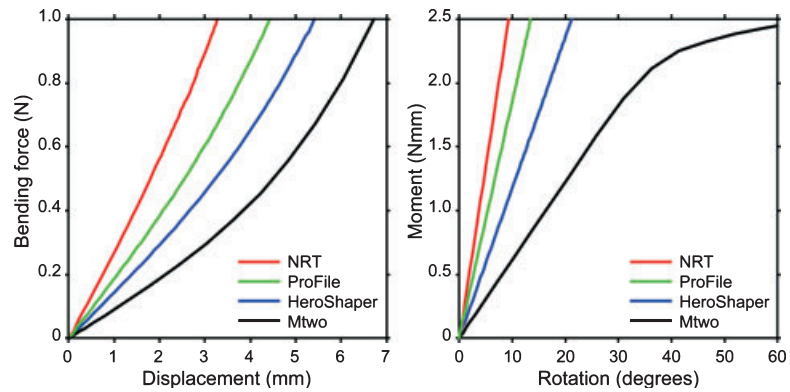


Figure 4 Left: flexure and von Mises stress distributions under the 1 N file tip loading. (a) ProFile with deflection of 4.59 mm and maximum stress of 577 MPa; (b) HeroShaper with deflection of 5.59 mm and maximum stress of 549 MPa; (c) Mtwo with deflection of 5.34 mm and maximum stress of 690 MPa; (d) NRT with deflection of 3.50 mm and maximum stress of 706 MPa. Right: flexure and stress distributions when the file tip was bent 2 mm. (a) ProFile with maximum stress of 274 MPa; (b) HeroShaper with maximum stress of 235 MPa; (c) Mtwo with maximum stress of 305 MPa; (d) NRT with maximum stress of 537 MPa.

von Mises equivalent stress values in the instruments were 537 MPa (NRT), 305 MPa (Mtwo), 274 MPa (ProFile) and 235 MPa (HeroShaper).

Figure 3 (right) shows the rotation–moment curves of the four systems. If rotational stiffness is defined as the moment needed for rotational deformation, a steeper slope indicates a higher stiffness. The graph shows that the NRT system had the highest rotational stiffness, whilst the Mtwo system was the least stiff (i.e. most compliant). The rotational stiffness curves were mostly linear, except for the Mtwo system at high torque values. It was verified that the nonlinearity was due mainly to geometrical factors within the investigated torque range. Figure 5 shows the von Mises stress distributions in a cross section for each instrument type during the torsion loads. The highest

maximum von Mises stresses were found close to the fixed cross section (4 mm from the tip). The highest maximum von Mises stress value in each system during simulation III (2.5 N mm torque) was found for Mtwo (860 MPa), followed by the HeroShaper (621 MPa), NRT (541 MPa) and ProFile (455 MPa). When a fixed 10° rotation angle was applied (simulation IV) the highest maximum von Mises stress was found for NRT (376 MPa) and followed by the ProFile (333 MPa), HeroShaper (300 MPa) and Mtwo (240 MPa).

Simulated canal shaping and residual stresses

The stresses in the four rotating instrument were also calculated whilst inserted in the simulated curved root canal. The stress distribution in the four instruments

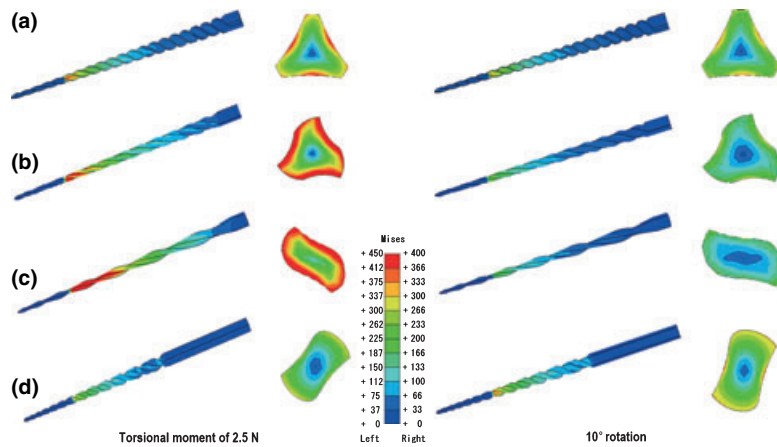


Figure 5 Left: von Mises stress distributions under a 2.5 N mm torsional moment. (a) ProFile with maximum stress of 455 MPa; (b) HeroShaper with maximum stress of 621 MPa; (c) Mtwo with maximum stress of 860 MPa; (d) NRT with maximum stress of 541 MPa. Right: stress distributions when file shafts were rotated 10°. (a) ProFile with maximum stress of 333 MPa; (b) HeroShaper with maximum stress of 300 MPa; (c) Mtwo with maximum stress of 240 MPa; (d) NRT with maximum stress of 376 MPa.

during their rotation at full depth in the simulated canal is shown in a longitudinal inner view in Fig. 6. The highest stresses were found at the surface of the bent section. The highest maximum von Mises stress values was found for the NRT (1474 MPa), followed by the Mtwo (1298 MPa), ProFile (905 MPa) and HeroShaper (810 MPa). Each 360° rotation within the simulated curved canal caused a reversal in bending direction. This is illustrated in Fig. 6, which plots the von Mises equivalent stress in the four instruments for one node at the instrument surface where the maximum von Mises stress was found. Note that the von Mises criterion does not distinguish between tensile and compressive stresses, therefore, the two extremes represent maximum bending in either direction. The table in Fig. 6 lists the maximum and minimum stress amplitudes (S_{max} and S_{min}), the stress difference ΔS ($S_{max} - S_{min}$) and R (S_{min}/S_{max}). The greatest stress difference (ΔS -value) during rotation was found for the Mtwo (1088 MPa), followed by the NRT (678 MPa), ProFile (457 MPa) and HeroShaper (262 MPa).

After the simulated shaping, the instruments were withdrawn from the curved root canal, allowing elastic recovery and the residual stress distributions along their length were examined (Fig. 7, upper set). The NRT model had the highest residual stresses (571 MPa), which exceeded the phase transformation stress of the NiTi alloy. The maximum residual von Mises stresses in the Mtwo, HeroShaper and ProFile were 448, 352 and 326 MPa respectively. Figure 7 also shows the resulting plastic deformation (lower set), which left the retracted instruments permanently bent. The permanent displacement of the file tips was calculated for the NRT, Mtwo, HeroShaper and ProFile as 366, 278, 187 and 138 μm respectively.

Discussion

Root canal instruments manufactured with NiTi alloys have been developed in an attempt to overcome the limitations of stainless steel alloys (Walia *et al.* 1988). NiTi instruments have two to three times higher elastic flexibility and a superior resistance to torsional fracture compared to similar-sized conventional stainless steel instruments (Glosson *et al.* 1995, Garip & Gunday 2001, Chen & Messer 2002, Schäfer *et al.* 2004). However, there is still a risk of NiTi instruments fracturing within root canals, which remains a matter of concern. It has been shown that cross-sectional geometry has a direct effect on the mechanical performance of NiTi instruments (Turpin *et al.* 2000, Berutti *et al.* 2003, Schäfer *et al.* 2003, Xu *et al.* 2006, Kim *et al.* 2008). Turpin *et al.* (2000) reported that cross-sectional configuration was the predominant factor for bending properties of NiTi instruments. Hayashi *et al.* (2007) concluded that bending loads of NiTi instruments with rectangle-based cross-sectional shapes were lower than those with triangle-based geometries.

The present study evaluated stress distributions under simulated loading and shaping, and compared residual stresses and plastic deformations after shaping of a curved canal by NiTi rotary instruments with various cross-sectional geometries. Of the four instruments that were evaluated in this study, ProFile and HeroShaper represented triangle shape-based designs which means that they have a repeating geometry every 120°. Mtwo with an S-shaped design and NRT represent rectangle-based cross sections which have a geometry that repeats every 180°.

The four instruments were compared in bending (simulations I and II) and torsion (simulations III and

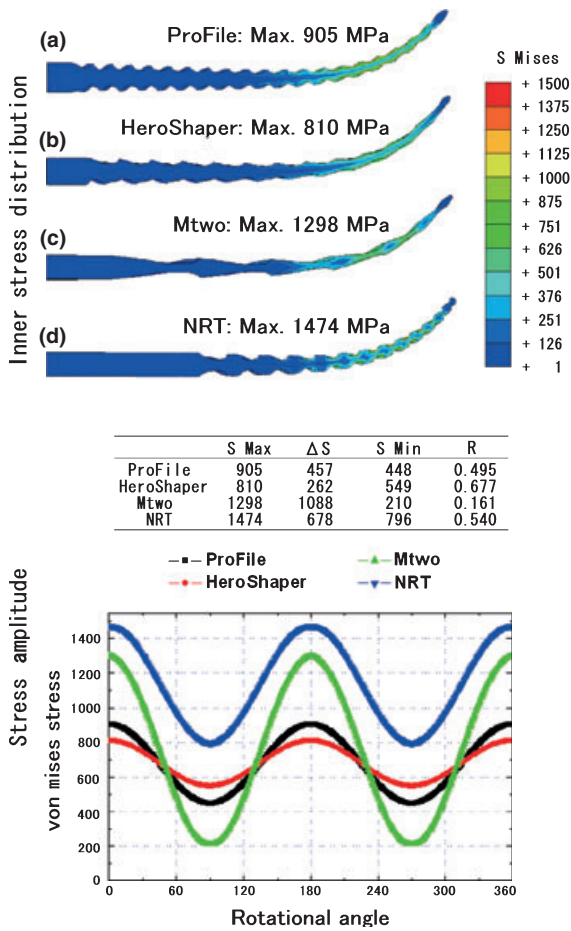


Figure 6 Internal von Mises stress distributions and cyclic stresses during simulated canal shaping in a curved canal. The cyclic stress values of each file were recorded at the node where the maximum von Mises stress was found. The maximum and minimum stress amplitudes along with the resulting $\Delta S (=S_{max} - S_{min})$ and $R (=S_{min}/S_{max})$ values are listed. Mtwo and NRT show bigger stress amplitudes than ProFile and HeroShaper.

IV) (Fig. 3). Bending stiffness characterizes the canal-following ability (i.e. the flexibility to easily follow the curvature of a canal), whilst torsional stiffness can be associated with cutting efficiency. The lowest bending stiffness was found for the Mtwo which also had a slightly smaller taper. This suggests that the Mtwo instrument would follow curved canals more easily than the other instruments. Higher deformation (in bending as well as torsion) will generally result in higher stresses. Figures 4 and 5 show that under the same load conditions (simulations I and III) the highest stresses are found in the more flexible Mtwo instrument. The NRT showed the highest stiffness, which

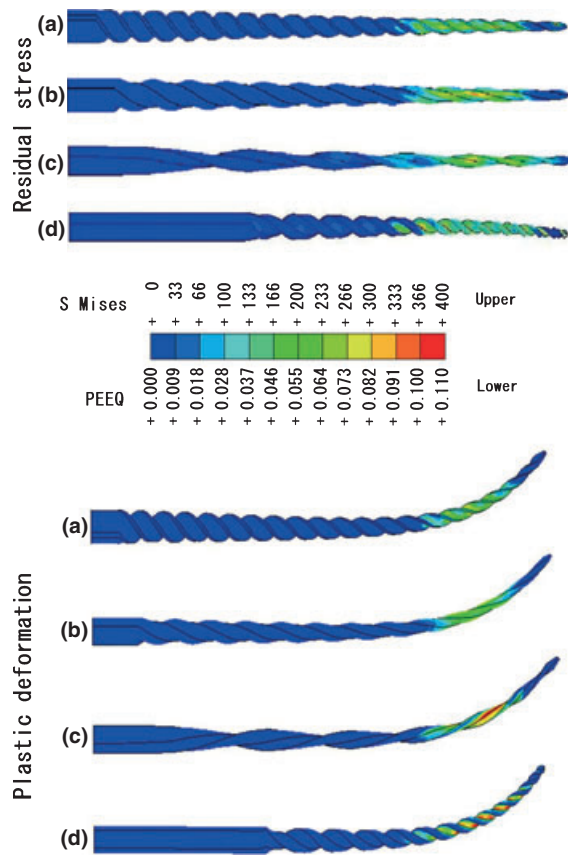


Figure 7 The upper set shows residual stress distributions after elastic recovery of the withdrawn files [maximum values: (a) ProFile 326 MPa; (b) HeroShaper 352 MPa; (c) Mtwo 448 MPa; (d) NRT 571 MPa] and shows the total permanent displacements (ProFile, 138 μm ; HeroShaper, 187 μm ; Mtwo, 278 μm ; NRT, 366 μm). The lower set shows the distribution of plastic deformation (von Mises strain) whilst still inside the curved canal [maximum values: (a) ProFile 0.08946; (b) HeroShaper 0.07421; (c) Mtwo 0.107321; (d) NRT 0.11066].

may be attributed to the shorter length of its working blade and long rigid shaft. Under the same bending deflection (simulation II), the highest stress concentrations were calculated for the NRT. This may have been expected, as the stiffer instrument requires a larger bending force to achieve the same deflection. However, stress depends not only on the applied forces but also on geometry. Although the Mtwo had the lowest stiffness and required the lowest bending force to attain the same deformation, the overall stresses in the stiffer HeroShaper and ProFile with triangular cross sections were lower than for the rectangle-based Mtwo (Fig. 4). This can be explained by the bending deformation of the Mtwo which was distributed across a smaller

cross-sectional area than the ProFile and HeroShaper systems. The more flexible Mtwo instrument bent and twisted more than the stiffer files, resulting in more deformation and thus higher stresses.

In the torsion tests, the clinical effect of instrument binding was simulated by fixing the instruments at 4 mm from the file tip. Two torsional conditions were prescribed; a constant torque of 2.5 N mm (simulation III) and a constant rotation of 10° (simulation IV). Analogies for the two torsion conditions, a prescribed torque or a prescribed rotation, are a pneumatic and electrical driving systems respectively. The highest stresses concentrated at the binding point (Fig. 5). Under a constant torque condition (simulation III), the FE simulation showed the highest stresses in the Mtwo, which had the lowest stress levels when a constant rotation (simulation IV) was prescribed. These rotational tests illustrate the rapid localized stress increase in a binding (taper-lock) area that increases the risk of fracture. As high torsional stresses may exceed the elastic limit, causing plastic deformation and fracture (Sattapan *et al.* 2000), binding during canal shaping should be avoided, for example by a torque-control system. The NRT, which had the highest torsional stiffness and longest rigid shank, had the highest maximum stress for the prescribed rotation of 10° (simulation IV). On the other hand, the Mtwo, with the smallest outside diameter of 5% taper and the lowest torsional stiffness, had the lowest maximum stress level for this condition (simulation IV). It can be concluded that the stress levels in the instruments could not be predicted by their stiffness response alone. The geometry of a cross section represents various factors that will affect the stress distribution, such as the cross-sectional area, polar moment of inertia, depth of the flute, area of the continuous inner core, radial land and peripheral surface ground. As the area of the inner core of the cross section increased, the model was more torque resistant (Xu *et al.* 2006). Yao *et al.* (2006) also noted that instruments with smaller diameters will fracture more readily. These were explained similarly by the simulation situation of 2.5 N mm of torsional rotation.

Stiffness (and its reciprocal flexibility) is not a material property, but depends on a combination of factors: geometry, mechanical properties of NiTi and boundary conditions, i.e. where the instrument is held, where the bending force is applied and where the deformation is measured. Instrument designs with equal length and taper profile can still have different stiffness values due to differences in cross-sectional geometry. Furthermore, the effective stiffness is likely to change when an

instrument is inserted into a canal because boundary conditions inside the canal vary due to changing contact points whilst the instrument is pushed along the curved canal walls. The canal-following ability, cutting efficiency and stresses of a file system can thus not be completely determined by a file's stiffness factors. To better study the effect of different cross sections on the mechanical performance, the instruments were tested inside a simulated curved canal during shaping.

File failure can be brought about by different fracture mechanisms. Superelastic properties allow relatively large bending of NiTi instruments before reaching the breaking point. However, repetitive loading can lead to fatigue crack initiation at stress levels below the failure strength. Fatigue failure is a major concern for NiTi instruments (Kuhn *et al.* 2001), particularly when used in curved canals. Figure 6 shows the resulting von Mises stresses created during those conditions, where tensile and compressive stresses alternate. Note that the von Mises criterion does not distinguish between compression and tension. Therefore, the two extremes represent maximum bending in either direction (i.e. a maximum compressive stress and minimum tensile stress may contribute to the von Mises stress value). The figure shows a different character for the two types of cross sections. The rectangle-based cross sections had high amplitudes, high ΔS , whilst the triangle-based instruments had low amplitudes. The higher stress ranges of Mtwo and NRT may indicate a higher fatigue propagation rate and thus a potentially higher fatigue failure risk (Cheung & Darvell 2007a, Kim *et al.* 2008). This high ΔS can be explained by the large difference in bending stiffness depending on the bending direction for a rectangular cross section. Bending stiffness is largest in the direction in which the cross-sectional height is greatest. In a triangular case, there is less difference between largest and smallest cross-sectional dimensions, hence a lower amplitude was found. According to the classic fatigue theory, fatigue crack growth is a function of ΔK (Paris & Erdogan 1963). K is the stress intensity factor, which represents the severity of the stress field in front of a crack. Assuming that this value can be compared with the general stress situation and considering existing fatigue crack propagation data (McKelvey & Ritchie 2001), the higher stress ranges of Mtwo and NRT in Fig. 6 may indicate a higher fatigue-crack propagation rate and thus potentially a higher fatigue failure risk.

In this study, residual stresses created by plastic deformation of the instruments in the simulated curved canal were also analysed after withdrawal (Fig. 7). A

change in the microstructure from austenite to martensite changes the mechanical properties, in particular an increase in elastic modulus and brittleness. The property changes caused by plastic deformation and the potential increase in stress levels due to residual stresses may effectively weaken an instrument, and should therefore be avoided. The level of residual stresses and amount of permanent deformation after the simulated shaping action was found to be higher for the Mtwo and NRT instruments with rectangle-based cross-sectional designs than for the ProFile and HeroShaper with triangular designs. Although geometrically realistic models of the instruments were used for this analysis, residual stresses and permanent deformation under clinical condition may differ from this simulation because of the assumed rigid canal and low coefficient of friction between canal and instrument.

This study investigated the effect of two basic cross-sectional geometries (triangle- and rectangle-based) for four instruments. Although the sizes of the instruments were selected to be as close to each other as possible, the comparison and thus conclusions about the effect of the cross-sectional features may still have been influenced by brand-dependent dimensional differences. To more definitively determine how the two types of basic cross-sectional geometries affect the mechanical response, a future numerical evaluation should be carried out for idealized file designs that only differ in the cross-sectional features.

Conclusion

The different cross-sectional designs of NiTi instruments resulted in different deformation responses during simulated bending and torsion loads. The main structural characteristics between the investigated systems were cross-sectional geometry, 120° or 180° repeating geometry and noncutting shaft length. NiTi rotary instruments with S-shaped and modified rectangular cross sections such as Mtwo or NRT created higher stress differentials during simulated shaping of curved canals and sustained more residual stress and deformation than the ProFile and HeroShaper instruments with triangle-based cross sections. Rectangle-based cross-sectional designs may have an increased fracture or fatigue risk.

References

Averbach RE, Kleier DJ (2001) Endodontics in the 21st century: the rotary revolution. *Compendium of Continuing Education in Dentistry* **22**, 27–34.

- Berutti E, Chiandussi G, Gaviglio I, Ibba A (2003) Comparative analysis of torsional and bending stresses in two mathematical models of nickel-titanium rotary instruments: ProTaper versus ProFile. *Journal of Endodontics* **29**, 15–9.
- Camps JJ, Pertot WJ (1994) Relationship between file size and stiffness of stainless steel instruments. *Endodontics and Dental Traumatology* **10**, 260–3.
- Camps JJ, Pertot WJ, Levallois B (1995) Relationship between file size and stiffness of nickel titanium instruments. *Endodontics and Dental Traumatology* **11**, 270–3.
- Chen JL, Messer HH (2002) A comparison of stainless steel hand and rotary nickel-titanium instrumentation using a silicone impression technique. *Australian Dental Journal* **47**, 12–20.
- Cheung GS, Darvell BW (2007a) Fatigue testing of a NiTi rotary instrument. Part 1: strain-life relationship. *International Endodontic Journal* **40**, 612–8.
- Cheung GS, Darvell BW (2007b) Fatigue testing of a NiTi rotary instrument. Part 2: fractographic analysis. *International Endodontic Journal* **40**, 619–25.
- Cheung GS, Shen Y, Darvell BW (2007) Effect of environment on low-cycle fatigue of a nickel-titanium instrument. *Journal of Endodontics* **33**, 1433–7.
- Garip Y, Gunday M (2001) The use of computed tomography when comparing nickel-titanium and stainless steel files during preparation of simulated curved canals. *International Endodontic Journal* **34**, 452–7.
- Glosson CR, Haller RH, Dove SB, del Rio CE (1995) A comparison of root canal preparations using Ni-Ti hand, Ni-Ti engine-driven, and K-Flex endodontic instruments. *Journal of Endodontics* **21**, 146–51.
- Hayashi Y, Yoneyama T, Yahata Y et al. (2007) Phase transformation behaviour and bending properties of hybrid nickel-titanium rotary endodontic instruments. *International Endodontic Journal* **40**, 247–53.
- Kazemi RB, Stenman E, Spångberg LS (2000) A comparison of stainless steel and nickel-titanium H-type instruments of identical design: torsional and bending tests. *Oral Surgery Oral Medicine Oral Pathology Oral Radiology and Endodontics* **90**, 500–6.
- Kim HC, Cheung GS, Lee CJ, Kim BM, Park JK, Kang SI (2008) Comparison of forces generated during root canal shaping and residual stresses of three nickel-titanium rotary files by using a three-dimensional finite-element analysis. *Journal of Endodontics* **34**, 743–7.
- Kim TO, Cheung GSP, Lee JM, Kim BM, Hur B, Kim HC (2009) Stress distribution of three NiTi rotary files under bending and torsional conditions using a mathematic analysis. *International Endodontic Journal* **42**, 14–21.
- Kuhn G, Tavernier B, Jordan L (2001) Influence of structure on nickel-titanium endodontic instruments failure. *Journal of Endodontics* **27**, 516–20.
- McKelvey AL, Ritchie RO (2001) Fatigue-crack growth behavior in the superelastic and shape-memory alloy

- Nitinol. *Metallurgical and Materials Transactions A* **32A**, 731–43.
- Paris P, Erdogan F (1963) A critical analysis of crack propagation laws. *Transactions of the ASME. Series D, Journal of Basic Engineering* **85**, 528.
- Peters OA (2004) Current challenges and concepts in the preparation of root canal systems: a review. *Journal of Endodontics* **30**, 559–67.
- Sattapan B, Nervo GJ, Palamara JE, Messer HH (2000) Defects in rotary nickel-titanium files after clinical use. *Journal of Endodontics* **26**, 161–5.
- Schäfer E, Tepel J (2001) Relationship between design features of endodontic instruments and their properties. Part 3. Resistance to bending and fracture. *Journal of Endodontics* **27**, 299–303.
- Schäfer E, Dzepina A, Danesh G (2003) Bending properties of rotary nickel-titanium instruments. *Oral Surgery Oral Medicine Oral Pathology Oral Radiology and Endodontics* **96**, 757–63.
- Schäfer E, Schulz-Bongert U, Tulus G (2004) Comparison of hand stainless steel and nickel titanium rotary instrumentation: a clinical study. *Journal of Endodontics* **30**, 432–5.
- da Silva FM, Kobayashi C, Suda H (2005) Analysis of forces developed during mechanical preparation of extracted teeth using RaCe rotary instruments and ProFiles. *International Endodontic Journal* **38**, 17–21.
- Thompson SA, Dummer PMH (1997) Shaping ability of ProFile.04 Taper Series 29 rotary nickel-titanium instruments in simulated root canals. Part 1. *International Endodontic Journal* **30**, 1–7.
- Turpin YL, Chagneau F, Vulcain JM (2000) Impact of two theoretical cross-sections on torsional and bending stresses of nickel-titanium root canal instrument models. *Journal of Endodontics* **26**, 414–7.
- Walia H, Brantley WA, Gerstein H (1988) An initial investigation of the bending and torsional properties of Nitinol root canal files. *Journal of Endodontics* **14**, 346–51.
- Wang GZ (2007) A finite element analysis of evolution of stress–strain and martensite transformation in front of a notch in shape memory alloy NiTi. *Materials Science and Engineering A* **460** **461**, 383–91.
- Xu X, Eng M, Zheng Y, Eng D (2006) Comparative study of torsional and bending properties for six models of nickel-titanium root canal instruments with different cross-sections. *Journal of Endodontics* **32**, 372–5.
- Yao JH, Schwartz SA, Beeson TJ (2006) Cyclic fatigue of three types of rotary nickel-titanium files in a dynamic model. *Journal of Endodontics* **32**, 55–7.

This document is a scanned copy of a printed document. No warranty is given about the accuracy of the copy. Users should refer to the original published version of the material.